Journal of ELECTRONIC MATERIALS, Vol. 37, No. 5, 2008
DOI: 10.1007/s11664-007-0350-y

Growth of Polarity-Controlled ZnO Films on (0001) Al_2O_3

J.S. PARK,[1,5] J.H. CHANG,[2] T. MINEGISHI,[1] H.J. LEE,[1] S.H. PARK,[1] I.H. IM,[1] T. HANADA,[1] S.K. HONG,[3,5] M.W. CHO,[1,4] and T. YAO[1,4]

1.—Institute for Materials Research, Tohoku University, Katahira 2-1-1, Aoba-ku, Sendai, Japan. 2.—Major of Semiconductor Physics, Korea Maritime University, Pusan, Republic of Korea. 3.—Department of Nano Information Systems Engineering, Chungnam National University, Daejeon, Republic of Korea. 4.—Center for Interdisciplinary Research, Tohoku University, Sendai, Japan. 5.—e-mails: jspark@imr.tohoku.ac.jp; soonku@cnu.ac.kr

The polarity control of ZnO films grown on (0001) Al_2O_3 substrates by plasma-assisted molecular-beam epitaxy (P-MBE) was achieved by using a novel CrN buffer layer. Zn-polar ZnO films were obtained by using a Zn-terminated CrN buffer layer, while O-polar ZnO films were achieved by using a Cr_2O_3 layer formed by O-plasma exposure of a CrN layer. The mechanism of polarity control was proposed. Optical and structural quality of ZnO films was characterized by high-resolution X-ray diffraction and photoluminescence (PL) spectroscopy. Low-temperature PL spectra of Zn-polar and O-polar samples show dominant bound exciton (I_8) and strong free exciton emissions. Finally, one-dimensional periodic structures consisting of Zn-polar and O-polar ZnO films were simultaneously grown on the same substrate. The periodic inversion of polarity was confirmed in terms of growth rate, surface morphology, and piezo response microscopy (PRM) measurement.

Key words: Polarity, PPZnO, interface, ZnO, nitrides, buffer layers

INTRODUCTION

ZnO is an attractive material for application in ultraviolet optoelectronic devices, due to its wide band gap of 3.37 eV and large exciton binding energy of 60 meV at room temperature.[1] ZnO crystallizes in a wurtzite crystal structure by the hexagonal close packing of Zn surrounded by four O in a tetrahedron with the vertex pointing along the ⟨0001⟩ direction. Wurtzite structure ZnO has crystal polarity due to the lack of inversion symmetry. Polarity affects the structural, chemical, optical, and electrical properties of ZnO layer.[2,3] Polarity is regarded as one of the important issues to be considered in the design of novel devices.[4,5] Various methods of polarity control are required for the development of new applications. To date, however, only a few methods have been reported for polarity control of ZnO films on c-sapphire substrates.[6–8] Kato et al. used the variation of thickness of MgO layers on sapphire substrates[6] and Wang et al. used well-defined ultrathin AlN layers formed by nitridation of sapphire substrate.[7] Although these methods are capable of selecting the polarity, careful process control is needed to ensure the desired polarity.

It is expected that a film with one- or two-dimensional polarity control would create a new application of ZnO for nonlinear optical devices. Already, impressive progress has been made on a nonlinear optical device made of $LiNbO_3$ and $LiTaO_3$ using a periodic array of polarity.[9,10] The authors previously reported that polarity control of ZnO was achieved by using Cr compound intermediate layers.[11] In that report, it was demonstrated that CrN could be applied not only for the growth of ZnO with high crystallinity, but also to provide a method for two-dimensional polarity control of ZnO films.

In this paper, a new approach for polarity control of ZnO films is reported in detail. The mechanism for the determination of polarity is proposed and the structural/optical properties of ZnO films are

(Received August 1, 2007; accepted November 5, 2007; published online November 30, 2007)

discussed. One-dimensional periodically poled ZnO (PPZnO) films are fabricated.

EXPERIMENTAL DETAILS

(0001) Al_2O_3 substrates were degreased in acetone and methanol for 10 min each at room temperature. Chemical etching was performed by using a H_2SO_4:H_3PO_4 = 3:1 solution at 160°C for 10 min. After the surface etching, the substrate was rinsed in deionized water for 1 min, then dried in a spin drier. Thermal treatment was performed in a III-nitride molecular-beam epitaxy (MBE) chamber for 10 min at 800°C. The CrN films were grown at 700°C by using a solid-source Cr effusion cell and nitrogen plasma. The samples were then transferred into a plasma-assisted II-oxide MBE chamber. Two ZnO samples were prepared: one grown on O-exposed CrN/Al_2O_3, the other grown on Zn-exposed CrN/Al_2O_3. O-exposure at 650°C for 10 min resulted in the formation of a Cr_2O_3 layer on the CrN/Al_2O_3 surface, while Zn-exposure prevented the formation of an oxide layer on the surface. The growth process was monitored by *in situ* reflection high-energy electron diffraction (RHEED) observation. ZnO films were grown at 700°C with a Zn beam flux of 0.14 nm/s, while the oxygen flow rate was 1 sccm with an radiofrequency (RF) power of 300 W. Details of the pretreatment and growth of the CrN layer are described elsewhere.[11]

The crystal structure and phase of each layer were investigated by high-resolution transmission electron microscopy (HRTEM) and diffraction pattern analysis. A Jeol JEM 3010 TEM operating at 300 keV was used for HRTEM. The crystal polarity of ZnO layers was determined based on the polarity dependence of wet etching and growth rates. Chemical wet etching was carried out using 0.01 M hydrochloric acid solution at room temperature and the etching rate was measured. High-resolution X-ray diffraction (HRXRD) was performed on the symmetric (0002) and asymmetric ($10\bar{1}2$) reflection planes to confirm the crystal quality of ZnO films. Low-temperature photoluminescence (PL) spectra were measured at 10 K using a He-Cd laser (325 nm) as an excitation source. Finally, one-dimensional PPZnO film was created by using stripe-patterned CrN buffer layers, 10 μm-wide, on Al_2O_3 substrate. This was designed to simultaneously grow Zn-polar ZnO on the CrN stripe pattern and O-polar ZnO on the Al_2O_3 surface. The periodical polarity control was confirmed by the measurement of surface morphology, the growth rate, and the voltage–piezo response (V–Z) curves.

RESULTS AND DISCUSSION

Effect of Zn Pre-exposure on ZnO Film Growth

Figure 1 shows the cross-sectional HRTEM micrograph of a ZnO film grown on the CrN/Al_2O_3 substrate. Digital diffraction patterns (DDPs)

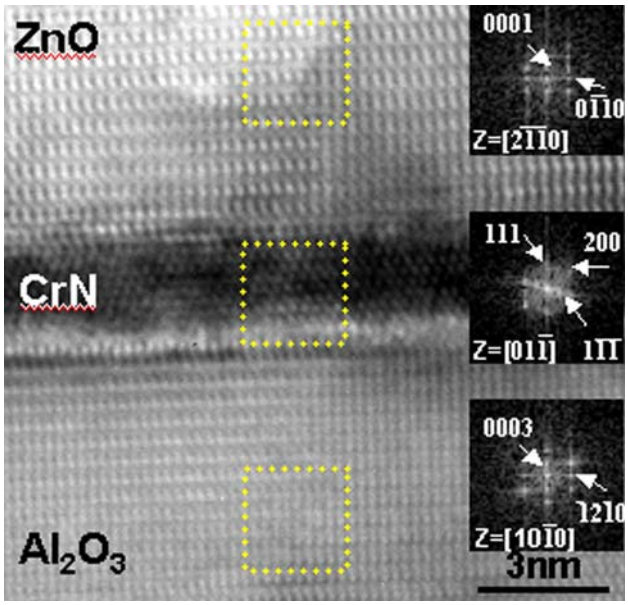

Fig. 1. Cross-sectional HRTEM micrograph of the ZnO/CrN/Al_2O_3. DDPs for the ZnO, CrN, and Al_2O_3 are shown on the right, and were obtained from the FFT of the marked square regions of the image.

obtained by fast Fourier transformation (FFT) of the HRTEM image are also shown in the figure. The DDPs were obtained from the square regions marked on the HRTEM image. Corresponding DDPs from ZnO and Al_2O_3 revealed the typical diffraction patterns of ZnO and Al_2O_3 for zone axes $\langle 11\bar{2}0\rangle$ and $\langle 10\bar{1}0\rangle$, respectively. Based on the camera constant determined from the DDPs for ZnO and Al_2O_3, the DDP from the CrN intermediate layer was indexed and determined to be the diffraction pattern for the rock-salt structure CrN with a $\langle 110\rangle$ zone axis. The calculated distances between the lattice planes along [200] and [111] directions in the CrN regions were d_{111} = 0.2364 ± 0.006 nm and d_{200} = 0.2060 ± 0.006 nm, respectively, which agreed reasonably well with the standard PDF values no. 65-9001 of 0.2072 nm and 0.2393 nm. The CrN layer was single crystalline with a thickness of 2.5 nm. Here, it should be noted that there was no additional oxide interfacial layer between the ZnO and CrN, which means the CrN layer was successfully protected from oxidation by the Zn-exposure before growing ZnO.[12] From the TEM study, the epitaxial relationship between ZnO, CrN, and Al_2O_3 was determined to be ZnO(0001)//CrN(111)//Al_2O_3(0001) and ZnO[$2\bar{1}\bar{1}0$]//CrN[$01\bar{1}$]//Al_2O_3[$10\bar{1}0$]. The orientation relationship was the same as the relationship determined from RHEED observations, as shown in Fig. 2. Twin structures are shown as CrN films grown on c-Al_2O_3, marked with a dot circle (Fig. 2b), and preserved during Zn exposure (Fig. 2c). The growth of ZnO on a Zn-exposed CrN surface resulted in an elongated, streaky RHEED pattern (Fig. 2d), which indicated that the initial ZnO growth was governed partly by a three-dimensional growth mode and partly by a

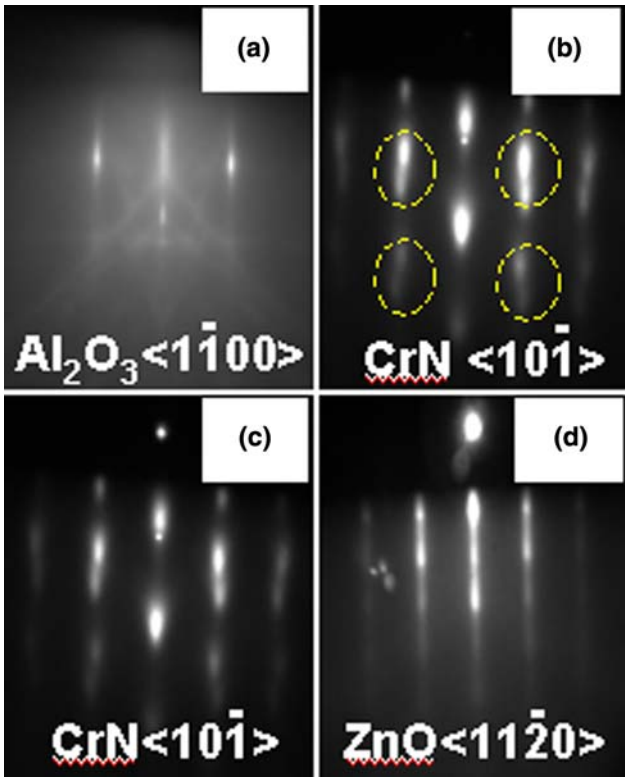

Fig. 2. RHEED patterns along $[11\bar{2}0]_{ZnO}$ electron-beam azimuths obtained from: (a) thermal cleaned Al_2O_3, (b) as grown CrN, (c) Zn-exposed CrN, and (d) HT-ZnO grown on Zn-exposed CrN.

layer-by-layer growth mode, which characterizes Zn-rich growth conditions.[13]

Effect of O Pre-exposure on ZnO Film Growth

Figure 3a shows the cross-sectional HRTEM micrograph for a ZnO film grown on an oxidized CrN/Al_2O_3 substrate. Two intermediate layers can be clearly seen between the ZnO and Al_2O_3. The DDPs for ZnO, Al_2O_3, and the two intermediate layers are shown in the inset of Fig. 3a. The lower intermediate layer was determined to be CrN based on the DDP analysis, as discussed above. The DDP from the upper intermediate layer was indexed and determined to have the diffraction pattern of rhombohedral structure Cr_2O_3 with a $\langle 01\bar{1}0\rangle$ zone axis. The calculated distances between the lattice planes along the [0001] and $[\bar{2}110]$ directions in the Cr_2O_3 regions on the CrN regions were $d_{\bar{2}110} = 0.2470 \pm 0.006$ nm and $d_{0003} = 0.4446 \pm 0.012$ nm, respectively, which were reasonably consistent with the standard PDF values no. 38-1479 of 0.2479 nm and 0.4531 nm.

The Cr_2O_3 layer was single crystalline with a thickness of 3.5 nm. Therefore, it was concluded that the top CrN layer was oxidized and successfully changed to a Cr_2O_3 layer, which was consistent with observations of RHEED patterns during oxidation of CrN film, as shown in Fig. 4.

Figure 4a shows the evolution of in-plane lattice constant during the formation of Cr_2O_3 on CrN/Al_2O_3. The azimuthal direction of the electron beam was parallel to the $[10\bar{1}]$ axis of CrN and the $[1\bar{1}00]$ axis of the Cr_2O_3 layer. RHEED patterns of CrN and Cr_2O_3 are shown in Fig. 4a. The in-plane lattice parameter of CrN (0.2930 nm) was used as a reference. The change in the in-plane lattice constant was consistent with the 30 degree rotated in-plane lattice constant of Cr_2O_3 obtained using the PDF values mentioned in the TEM analysis.

Contrary to Zn exposure, the RHEED pattern of the CrN surface became streaky when O plasma impinged onto the CrN surface, as shown in the inset of Fig. 4a. After the onset of the growth of HT ZnO films, the RHEED pattern was streaky (Fig. 4b), which indicated two-dimensional layer-by-layer growth. From the TEM and RHEED patterns, the epitaxial relationship between the layers was determined to

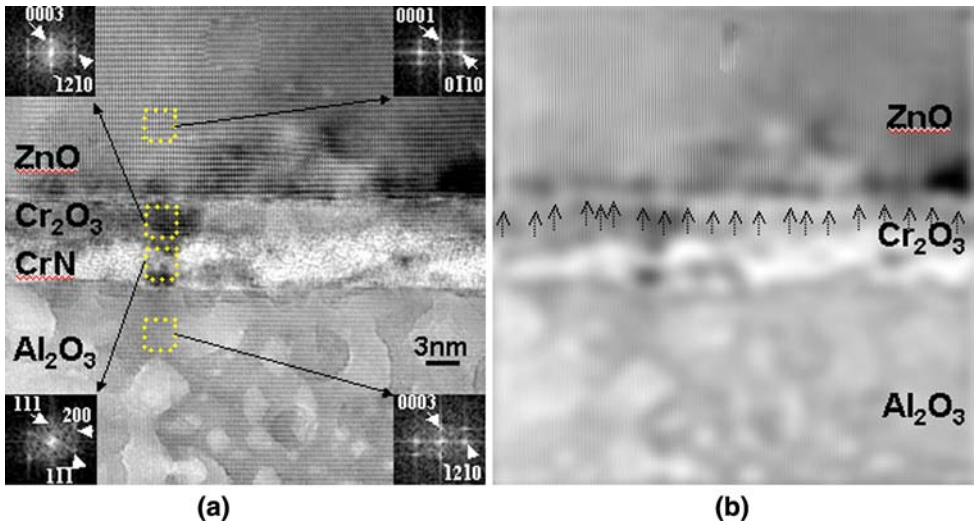

Fig. 3. (a) Cross-sectional HRTEM micrograph of ZnO/Cr_2O_3/CrN/Al_2O_3. DDPs for the ZnO, Cr_2O_3, CrN, and Al_2O_3 layers are shown in the inset, and were obtained from the FFT of the marked square regions of the image. (b) Inverse FFT filtered image showing the misfit dislocations at the ZnO/Cr_2O_3 interface.

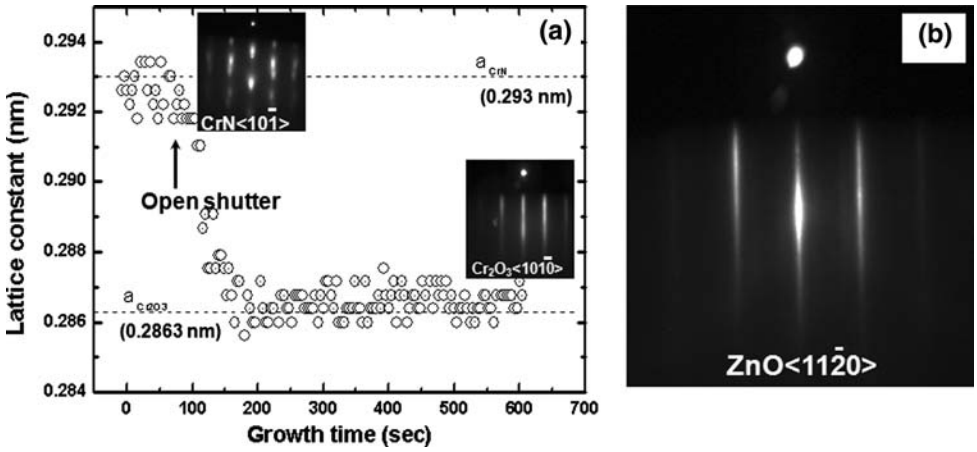

Fig. 4. (a) The evolution of in-plane lattice constant during the growth of Cr_2O_3 on CrN/Al_2O_3, with the azimuthal direction of the electron beam parallel to [10$\bar{1}$] CrN and [1$\bar{1}$00] Cr_2O_3. The RHEED patterns of CrN and Cr_2O_3 are shown. (b) The HT-ZnO RHEED pattern along [11$\bar{2}$0] grown on Cr_2O_3/CrN.

be as follows: ZnO(0001)//Cr_2O_3(0001)//CrN(111)// Al_2O_3(0001) and ZnO[2$\bar{1}\bar{1}$0]//Cr_2O_3[10$\bar{1}$0]//CrN[01$\bar{1}$]// Al_2O_3[10$\bar{1}$0]].

Misfit dislocations at the ZnO//Cr_2O_3 interface were clearly observed, as shown in Fig. 3b. The sums of the interplanar spacing for the seven and eight (0$\bar{1}$10) ZnO planes were 0.197 nm and 0.223 nm, and those for the eight and nine ($\bar{1}$2$\bar{1}$0) Cr_2O_3 planes were 0.198 nm and 0.225 nm. Therefore, the equilibrium spacing of the misfit dislocations at the ZnO/Cr_2O_3 interface can be predicted to be one misfit dislocation per every eight or nine Cr_2O_3 planes. Figure 3b shows a Fourier-filtered image using the (0$\bar{1}$10) and ($\bar{1}$2$\bar{1}$0) reflections for ZnO and sapphire, respectively. As marked by the arrows in Fig. 3b, on average one misfit dislocation was found per every eight or nine Cr_2O_3 planes at the interface, which implies domain-matching epitaxy.[14]

Evaluation of Polarity

In this experiment, the polarity of ZnO films was determined by investigating the differences in etching rate, growth rate, surface morphology, and PRM measurement.

Mariano and Hanneman reported different etching rates of opposite polar directions, based on a surface-bonding model for A_{II}-B_{VI}.[15] The layer of zinc surface atoms has a positive charge, while the layer of oxygen surface atoms has a negative charge with two dangling electrons due to the transfer of electrons of zinc atoms to the oxygen atoms. The dangling electrons on the O-polar surface account for the higher etching rate, due to the susceptibility to reaction of dangling bonds with electron-seeking agents in the etchant.[15] Such differences in chemical wet etching rates depending on the polarity of wurtzite structure materials have been reported in III-nitrides[16,17] and in ZnO,[18,19] which implies that polarity determination based on the wet etching rate is highly reliable.

In order to measure the etching rate accurately, a photoresist masking procedure was used. The sample was partially masked by photoresist, and wet etching was performed on the unmasked region of the sample. The mask was removed after etching, and the etching rate was determined by measuring the height of a step formed on the surface of ZnO film, using a surface profiler.

Chemical wet etching rates of the ZnO films grown on CrN/Al_2O_3 and Cr_2O_3/CrN Al_2O_3 were determined to be 10 nm/min and 95 nm/min, respectively. This indicated an etching rate about ten times higher for the ZnO film grown on Cr_2O_3. Such a remarkable difference in wet etching rate clearly indicates that ZnO films grown on CrN is Zn-polar and ZnO films grown on Cr_2O_3 have an O-polar surface.

In addition to the polarity dependence of the etching rate, differences in growth rate can be used to determine the polarity of ZnO films.[8,20] In general, the growth rate of Zn-polar ZnO is known to be 1.5 times higher than that of O-polar films. The higher growth rate of Zn-polar ZnO film can be understood in terms of the higher sticking coefficient of adatoms on the O-covered Zn-polar surface.[20] Each oxygen atom on a Zn-polar surface has three dangling bonds, while each oxygen atom on an O-polar surface has only one dangling bond, so the Zn sticking coefficient of the O-covered Zn-polar surface is larger than that of the O-polar surface. As a result, Zn-polar ZnO film has a higher growth rate.[20] In this experiment, the growth rates of the ZnO films grown on CrN/Al_2O_3 and $Cr_2O_3/CrN/Al_2O_3$ were 5.0 nm/min and 3.4 nm/min, respectively. Therefore, the higher growth rate for the ZnO film on CrN clearly indicates Zn-polar growth.

Mechanism of Polarity Selection

Figure 5a and b show schematics of the atomic arrangements of ZnO on CrN and Cr_2O_3, respec-

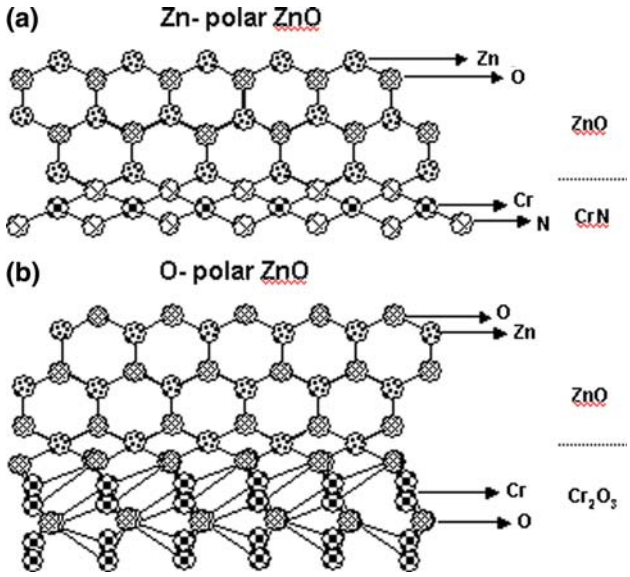

Fig. 5. Schematic picture of the atomic arrangements of the ZnO on (a) the CrN and on (b) the Cr_2O_3, resulting in Zn-polar and the O-polar ZnO films, respectively.

tively. The CrN surface is mostly N-terminated because the CrN growth was conducted under N-rich growth conditions. In the initial growth of ZnO on a CrN, Zn-exposure was employed to prevent oxidation of the CrN. Therefore, N-Zn bonding was expected at the interface, which was confirmed by XPS (data not shown). Since the topmost N atoms in rock-salt CrN have three dangling bonds, each Zn atom bonded with N atoms has only a single dangling bond along the growth direction, and each O atom bonding to the Zn atoms has three dangling bonds. As a result, the ZnO films on the CrN showed Zn-polarity, as shown in Fig. 5a. On the other hand, in the case of Cr_2O_3, an oxygen-terminated surface was expected based on the reported surface phase diagram as a function of oxygen partial pressure and temperature.[21] α-Cr_2O_3 has the corundum structure of space group $R\bar{3}c$ with hexagonal close-packed (0001) layers of O atoms, and two-thirds of the octahedral interstitial sites filled by Cr atoms.[22] Zn atoms at the interface will occupy octahedral sites bonding to three underlying oxygen atoms in the oxygen layer of Cr_2O_3. Oxygen atoms then bond to the Zn atoms while occupying the tetrahedral sites of ZnO, similar to AlN formation on the O-terminated (0001) Al_2O_3 by nitridation.[23] Therefore, every oxygen atom has one dangling bond along the c-direction, which results in O-polarity. As a result, the ZnO films on Cr_2O_3 had O-polarity.

Structural and Optical Qualities of ZnO Films Grown on Cr Compounds

The (0002) and (10$\bar{1}$2) ω-scans of both Zn-polar (on CrN/Al_2O_3) and O-polar (on Cr_2O_3/CrN/Al_2O_3) ZnO layers were measured by using HRXRD. The full width at half-maximum (FWHM) values of (0002) and (10$\bar{1}$2) ω-scans for Zn-polar ZnO are 504 arcsec and 720 arcsec, while those for O-polar ZnO are 576 arcsec and 1116 arcsec, respectively. The FWHM values for Zn-polar ZnO film are narrower than those for O-polar ZnO film. However, this does not simply mean that the crystallinity of Zn-polar film is better than that of O-polar film, since the difference in growth rates under the same growth conditions are used as proof of the polarity of grown film. The two ZnO samples were grown under nearly the same growth conditions. The resultant thicknesses for Zn- and O-polar ZnO films were estimated to be 320 nm and 210 nm, respectively. This strongly supports the determined polarity of the films as mentioned above, and also implies that the narrow FWHM of Zn-polar ZnO film should be attributed to the crystal size effect.[24] Moreover, it should be noted that serious deterioration of crystal quality of the ZnO films in terms of the FWHM of the XRD rocking curve was not observed. The XRD FWHMs of ZnO films grown on CrN layers are comparable to those of ZnO films grown on sapphire substrate using MgO buffer layers,[25] although the growth conditions were not optimized yet.

Figure 6 shows the low-temperature (10 K) PL spectra on a logarithmic scale for (a) O-polar and (b) Zn-polar ZnO films, respectively. The PL spectra of both samples could be characterized by strong near-band-edge emissions with very weak deep-level emissions. Strong ground-state free exciton emission (FX) was observed at 3.375 eV and at 3.374 eV from the O-polar and Zn-polar ZnO films, respectively. The FX position of O-polar ZnO was a little higher than the reported value of highly crystalline bulk ZnO (FX = 3.374 eV at 4.2 K).[26] This implies that O-polar ZnO film is under residual compressive strain, while Zn-polar ZnO is almost strain free at low temperature. The LT PL spectra are dominated

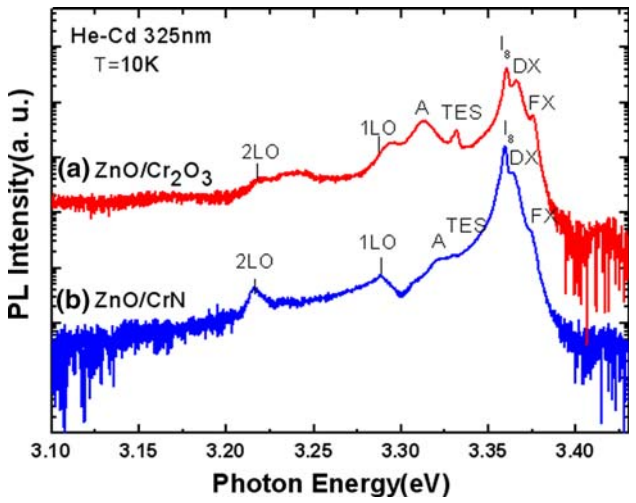

Fig. 6. Low-temperature PL spectra measured at 10 K of ZnO films grown on (a) Cr_2O_3/CrN buffer and (b) CrN.

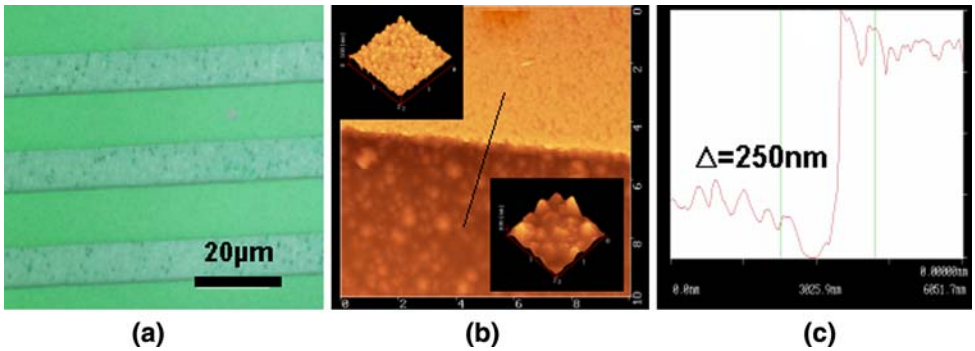

Fig. 7. (a) Optical microscopy image of PPZnO film grown on a 10 μm stripe-patterned CrN buffer layer. (b) A 2 μm $\times$ 2 μm AFM surface image of PPZnO and detailed surface morphology is shown in the inset. (c) Height profile of PPZnO films as marked with a solid line in (b).

by bound excitons in the range of 3.3660–3.3310 eV. The peak at the highest energy was assigned as a donor-bound exciton (D^0X). The peak was positioned at 3.3660 eV for O-polar ZnO and 3.3643 eV for Zn-polar ZnO. Those values appeared considerably higher than the commonly observed I_4 line (3.3628 eV), but were still lower than the peak position of the I_3 line (3.3665 eV). However, since they were in the spectral range for donor-bound excitons, they were temporarily assigned as D^0X.

The peak with the strongest intensity was observed at 3.3605 eV (O-polar ZnO), and at 3.3597 eV (Zn-polar ZnO), which corresponded well with the reported position for the I_8 line (3.3597 eV). The small discrepancy of O-polar ZnO was attributed to the effect of residual strain. The lowest emission line at around 3.331 eV was assigned to an emission related to a structural defect[27] such as Y-line recombination in ZnSe films.[28] The origin of a peak labeled "A" in Fig. 6 is unclear and under discussion.[29] However, it should be noted that the optical quality of both samples was very good.

The described structural/optical qualities of ZnO films suggest the feasibility of Cr compound buffer layers not only for polarity control, but also for the growth of high-quality ZnO films.

Demonstration of One-Dimensional PPZnO

Figure 7a shows optical microscopy images of periodically poled ZnO (PPZnO) grown on 10 μm stripe-patterned CrN buffer layers. Polarity-controlled ZnO films were successfully grown with 10 μm periodicity. Atomic force microscopy (AFM) images (Fig. 7b) clearly show the periodic variation of surface morphology and growth rate (Fig. 7c). ZnO films grown above CrN stripe patterns showed hexagonal pits, while hexagonal hillocks were observed from the ZnO films grown on the Al_2O_3 area. Those features are known as typical morphologies of Zn- and O-polar surfaces.[18,19] Also, the surface profile of the one-dimensional PPZnO clearly revealed the growth rate difference between the ZnO films grown on the CrN pattern and on the Al_2O_3 area. The estimated thickness for the ZnO films on CrN stripe patterns was about 700 nm, which is almost 1.5 times higher than that on the Al_2O_3 area. The surface *V–Z* curves of ZnO films are shown in Fig. 8. The piezo response microscopy (PRM) technique has previously been adopted to determine polarity in GaN.[30] It clearly shows opposite hysteresis piezo response curves with input voltage variation. The hysteresis curve for the ZnO films on the CrN patterns implies Zn-polarity, while

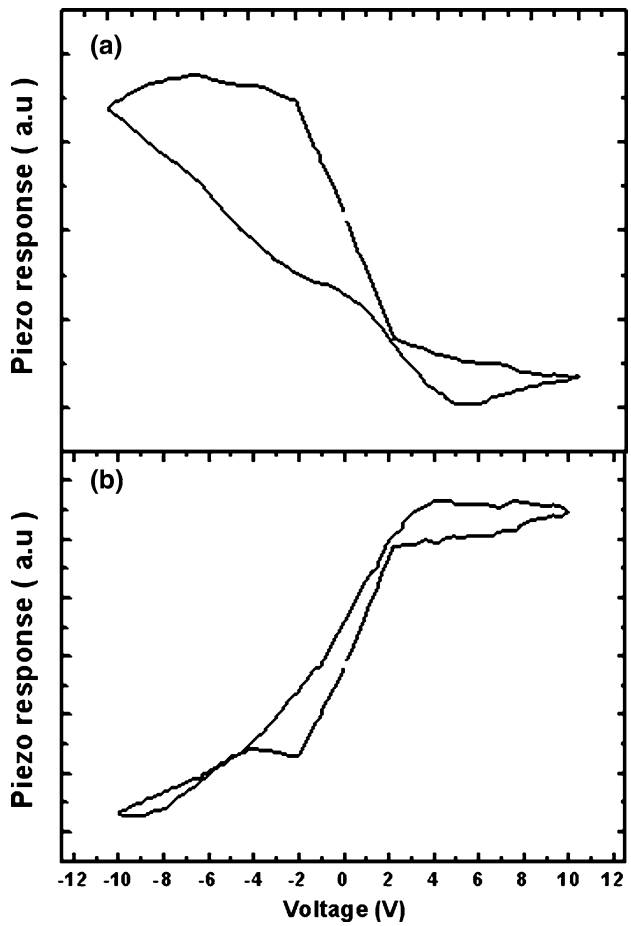

Fig. 8. Voltage–piezo response curve (*V–Z*) of ZnO film grown on patterned CrN: (a) Zn-polar ZnO and (b) O-polar ZnO film.

the hysteresis curve for ZnO films on the Al_2O_3 area indicates O-polarity. Therefore, we concluded that the ZnO films on the CrN stripe patterns and the Al_2O_3 area have Zn- and O-polar surfaces, respectively. This result successfully demonstrates the growth of one-dimensional PPZnO film on a substrate.

SUMMARY

The polarity of ZnO films on (0001) Al_2O_3 was controlled by using Cr-compound intermediate layers. Periodic polarity-controlled ZnO was successfully grown on a patterned CrN buffer layer. The experimental results can be summarized as follows.

(1) The Zn-polar ZnO films can be grown on CrN/Al_2O_3 without oxide layer formation through Zn-exposure on a CrN buffer layer. The epitaxy relationship is determined by RHEED and TEM as follows: ZnO(0001)//CrN(111)//Al_2O_3(0001) and ZnO[$2\bar{1}\bar{1}0$]//CrN[$01\bar{1}$]//Al_2O_3[$10\bar{1}0$].
(2) The growth of O-polar ZnO films was obtained by the formation of a Cr_2O_3 layer CrN/Al_2O_3. The epitaxy relationship is as follows: ZnO(0001)//Cr_2O_3(0001)//CrN(111)//Al_2O_3(0001) and ZnO[$2\bar{1}\bar{1}0$]//Cr_2O_3[$10\bar{1}0$]//CrN[$01\bar{1}$]//Al_2O_3[$10\bar{1}0$].
(3) Possible interface bonding models are proposed to explain the mechanism for polarity control on rock-salt CrN and rhombohedral Cr_2O_3 buffer layers on Al_2O_3(0001).
(4) Structural/optical properties reveal the feasibility of Cr-compound buffer layers, not only for polarity control, but also for the growth of high-quality ZnO layers.
(5) The simultaneous growth of Zn-/O-polar ZnO films was demonstrated by using stripe-patterned CrN buffer layers on an Al_2O_3 substrate.

ACKNOWLEDGEMENTS

J.S. Park appreciates the financial support for a Research Fellowship and a Grant-in-Aid from the Japan Society for the Promotion of Science (JSPS). S.K. Hong gratefully acknowledges support by a Korea Research Foundation Grant funded by the Korean Government (MOEHRD, Basic Research Promotion Fund) (KRF-2005-205-D00078).

REFERENCES

1. D.M. Bagnall, Y.F. Chen, Z. Zhu, S. Koyama, M.Y. Shen, T. Goto, and T. Yao, *Appl. Phys. Lett.* 70, 2230 (1997).
2. S.A. Chevtchenko, J.C. Moore, U. Ozgur, X. Gu, A.A. Baski, H. Morkoc, B. Nemeth, and J.E. Nause, *Appl. Phys. Lett.* 89, 182111 (2006).
3. S.K. Hong, T. Hanada, H.J. Ko, Y. Chen, D. Imai, K. Araki, M. Shinohara, K. Saitoh, M. Terauchi, and T. Yao, *Phys. Rev. B* 65, 115331 (2002).
4. J. Cai and F.A. Ponce, *J. Appl. Phys.* 91, 9856 (2002).
5. H. Tampo, H. Shibat, K. Matsubara, A. Yamada, P. Fons, S. Niki, M. Yamagata, and H. Kanie, *Appl. Phys. Lett.* 89, 132113 (2006).
6. H. Kato, K. Miyamoto, M. Sano, and T. Yao, *Appl. Phys. Lett.* 84, 4562 (2004).
7. Y. Wang, X.L. Du, Z.X. Mei, Z.Q. Zeng, M.J. Ying, H.T. Yuan, J.F. Jia, Q.K. Xue, and Z. Zhang, *Appl. Phys. Lett.* 87, 051901 (2005).
8. T. Minegishi, J.H. Yoo, H. Suzuki, Z. Vashaei, K. Inaba, K.S. Shim, and T. Yao, *J. Vac. Sci. Technol. B* 23, 1286 (2005).
9. S. Zhu, H. Zhu, and N. Ming, *Science* 279, 843–846 (1997).
10. A. Bruner, P. Shaier, and D. Eger, *Opt. Exp.* 14, 9371 (2006).
11. J.S. Park, S.K. Hong, T. Minegishi, S.H. Park, I.H. Im, T. Hanada, M.W. Cho, and T. Yao, *Appl. Phys. Lett.* 90, 201907 (2007).
12. S.K. Hong, T. Hananda, Y. Chen, H.J. Ko, T. Yao, D. Imai, K. Araki, and M. Shinohara, *Appl. Surf. Sci.* 190, 491 (2002).
13. H.J. Ko, T. Yao, Y. Chen, and S.K. Hong, *J. Appl. Phys.* 92, 4354 (2002).
14. J. Narayan and B.C. Larson, *J. Appl. Phys.* 93, 278 (2003).
15. A.N. Mariano and R.E. Hanneman, *J. Appl. Phys.* 34, 384 (1963).
16. D. Zhuang and J.H. Edgar, *Mater. Sci. Eng. R-Rep.* 48, 1 (2005).
17. A.R. Smith, R.M. Feenstra, D.W. Greve, M.-S. Shin, M. Skowronski, J. Neugebauer, and J.E. Northrup, *Appl. Phys. Lett.* 72, 2114 (1998).
18. X. Wang, Y. Tomita, O.H. Roh, M. Ohsugi, S.B. Che, T. Ishtani, and A. Yoshikawa, *Appl. Phys. Lett.* 86, 011921 (2005).
19. H. Tampo, P. Fons, A. Yamada, K.K. Kim, H. Shibata, K. Matsubara, S. Niki, H. Yoshikawa, and H. Kanie, *Appl. Phys. Lett.* 87, 141904 (2005).
20. H. Kato, M. Sano, K. Miyamoto, and T. Yao, *J. Cryst. Growth* 265, 375 (2004).
21. X.G. Wang and J.R. Smith, *Phys. Rev. B* 68, 201402 (2003).
22. C. Rehbein, N.M. Harrison, and A. Wander, *Phys. Rev. B* 54, 14066 (1996).
23. Z.X. Mei, Y. Wang, X.L. Du, M.J. Ying, Z.Q. Zeng, H. Zheng, J.F. Jia, Q.K. Xue, and Z. Zhang, *J. Appl. Phys.* 96, 7108 (2004).
24. G. Bauer and W. Richer, *Optical Characterization of Epitaxial Semiconductor Layers* (Berlin: Springer, 1983), Chapter 6.
25. H. Kato, M. Sano, K. Miyamoto, and T. Yao, *J. Cryst. Growth* 275, 2459 (2005).
26. K. Thonke, Th. Gruber, N. Teofilov, R. Schonfelder, A. Waag, and R. Sauer, *Phys. B* 308–310, 945 (2001).
27. P.J. Dean, *Phys. Stat. Sol. (a)* 81, 625 (1984).
28. B.K. Meyer, H. Alves, D.M. Hofmann, W. Kriegseis, D. Forster, F. Bertram, J. Christen, A. Hoffmann, M. Straβburg, M. Dworzak, U. Haboeck, and A.V. Rodina, *Phys. Stat. Sol. (b)* 241, 231 (2004).
29. A. Teke, U. Ozgur, S. Dogan, X. Gu, H. Morkoc, B. Nemeth, J. Nause, and H.O. Everitt, *Phys. Rev. B* 70, 195207 (2004).
30. B.J. Rodriguez, A. Gruverman, A.I. Kingon, R.J. Nemanich, and O. Ambacher, *Appl. Phys. Lett.* 80, 4166 (2002).